J Mater Sci: Mater Med (2007) 18:2319–2329
DOI 10.1007/s10856-007-3136-0

Mechanical characterization of dense calcium phosphate bioceramics with interconnected porosity

Y. H. Hsu · I. G. Turner · A. W. Miles

Received: 20 April 2006 / Accepted: 25 July 2006 / Published online: 14 June 2007

Abstract Porous hydroxyapatite/tricalcium phosphate (HA/TCP) bioceramics were fabricated by a novel technique of vacuum impregnation of reticulated polymeric foams with ceramic slip. The samples had approximately 5–10% interconnected porosity and controlled pore sizes appropriate to allow bone ingrowth, combined with good mechanical properties. A range of polyurethane foams with 20, 30 and 45 pores per inch (ppi) were used as templates to produce samples for testing. The foams were inpregnated with solid loadings in the range of 60–140 wt%. The results indicated that the average apparent density of the HA/TCP samples was 2.48 g/cm^3, the four-point bending strength averaged 16.98 MPa, the work of fracture averaged 15.46 J/m^2 and the average compressive strength was 105.56 MPa. A range of mechanical properties resulted from the various combinations of different grades of PU foam and the solid loading of slips. The results indicated that it is possible to manufacture open pore HA/TCP bioceramics, with compressive strengths comparable to human bone, which could be of significant clinical interest.

Introduction

Bioceramics are currently used in a range of applications including reconstructive, orthopaedic, otologic, maxillofacial, craniofacial and dental procedures [1, 2]. However, up until now, the hydroxyapatite (HA) and tricalcium phosphate (TCP) bioceramics developed have had isolated porosity, which constrains potential for bone ingrowth, or have had poor mechanical properties such that they could not be used for substantial load-bearing applications.

Porous calcium phosphate based ceramics are attractive for use as synthetic bone graft substitutes allowing successful tissue ingrowth, which further enhances the implant-tissue attachment [3–7]. The degree of interconnectivity and the nominal pore size are critical factors that determine the success of the implants. It is generally accepted that a minimum pore size of 100 μm is necessary for the porous implant materials to function well and a pore size greater than 200 μm is an essential requirement for osteoconduction. Research has also suggested that the degree of interconnectivity is more critical than the pore size [8, 9]. However, it is well known that the mechanical strength of a material generally decreases as its porosity increases. Conflicting interests exist between biological and mechanical requirements, thus the design of porous implant materials with a sufficient degree of interconnected porosity combined with optimal mechanical properties is an important challenge. A balance must be reached depending on the type of repair, rate of remodelling and rate of degradation of such scaffold materials [10].

Many methods have been developed to fabricate porous ceramics [6], including organic particle embedding techniques [11], production of gas bubbles in slips and the replication of reticulated porous structures [5]. However, these methods may be regarded as unsatisfactory in that they may fail to meet either or both of the two main demands which are: an adequate degree of interconnected porosity and optimal mechanical properties.

The main aim of this study was to fabricate dense but porous calcium phosphate bioceramics with completely interconnected porosity combined with good mechanical

Y. H. Hsu · I. G. Turner (✉) · A. W. Miles
Centre for Orthopaedic Biomechanics, Department of Mechanical Engineering, University of Bath, Claverton Down, Bath BA2 7AY, UK
e-mail: I.G.Turner@bath.ac.uk

properties to enable their use in substantial load-bearing applications.

Experimental procedure

Materials and methods

Two grades of calcium phosphate powder, TCP 118 and TCP 130 (Stryker Howmedica Osteonics), were used in this study. Varying the blend ratios of TCP 118 and TCP 130, and controlling the sintering temperature, changes the ratios of HA and TCP in the processed samples. This allows a balance between the long-term stability associated with HA and the relatively high solubility and bioactivity associated with TCP.

The organic reticulated foams, which were completely burnt out during sintering comprised polyurethane (PU) that had one of three different pores per inch (ppi)—20, 30 and 45 ppi (Sydney Heath and Sons Ltd.). The PU foams were sectioned using a scalpel and scissors to the desired shape and dimensions to be used as templates, then soaked in water for 24 h. This stage of the process removed dust and impurities from the foams.

Manufacturing process

To investigate the effect of solid loading on mechanical properties of the resulting samples, slips based on loadings of 600, 800, 1,000, 1,200 and 1,400 g of powder per litre (60–140 wt%) were prepared. The addition of the dispersing agent, Dispex A40, (Ammonium polyacrylate, Ciba, England) controlled the slip viscosity and improved the flow properties without decreasing the solid loading. For slips with higher solid loadings large amounts of dispersant were added, otherwise the slips were too thick to mill. While stirring, TCP 118 and TCP 130 powders (1:1) were gradually added in different proportions to distilled water in order to achieve various solid-loading levels in the slips. After adding the required amounts of powder, the mixtures were ball milled in polyethylene jars, using ZrO_2 balls as the milling media, for 24 h. This process improves the rheological properties of the suspensions and the packing ability during consolidation.

A high solid loading is required for greater density, improved mechanical properties, and minimal shrinkage in the final sintered product. However, the slip with a high solid loading has a high viscosity causing difficulty with impregnation and thus requires more dispersant. After ball milling, more dispersant was added to adjust the slip to an exact viscosity. The viscosity characteristics of the slip were measured using a Brookfield viscometer via a constant spindle speed of 10 rpm using a No. 5 spindle. The viscosity of the slip must be sufficiently low to allow it to enter and fill the foams, however, it should also be high enough to avoid the ceramic slip draining from the foam. Hence, the slip was vacuumed for 10 min before impregnation to remove any entrapped air bubbles which could decrease the density and compromise the mechanical strength of the bioceramics.

The foams were substantially impregnated with ceramic slip by a vacuum impregnation method as described in an earlier publication [12]. An important feature of the method is that the slip substantially fills the foams as opposed to only coating the walls. In the latter case, the resulting product would be a replica of the reticulated foam material and the ceramic parts of the structure would be hollow and therefore less strong. For comparative purposes, high density, solid samples were also produced from 100 wt% solid loading by slip casting. The ceramic slip was prepared in the same way as for vacuum impregnation, poured into a mould and dried for several days. All the dried green samples, both porous and dense were sintered at 1,280 °C. The final composition of the sintered samples was 75% HA and 25% TCP. Table 1 shows the range of samples produced from selected solid loadings and different ppi foams for experimental purposes.

Measurement of physical and mechanical properties

Density

The apparent densities of the samples were determined by a geometric wt/vol method. Six to eight specimens were used to determine the average density for each sample group.

Mechanical testing

Samples for mechanical testing were prepared as shown in Fig. 1. Large blocks of dimensions 45 × 45 × 17 mm were made, then sectioned to give smaller bars of 45 × 5 × 4 mm for four-point bending tests. After the bending test, the

Table 1 Samples for physical and mechanical properties measurement

	Foam size (ppi)		
Solid loading (wt%)	20 ppi	30 ppi	45 ppi
60	X	–	–
80	X	X	–
100	X	X	X
120	X	X	X
140	X	–	–
*Solid (slip cast)		X	

X = Tested

– = Non-tested

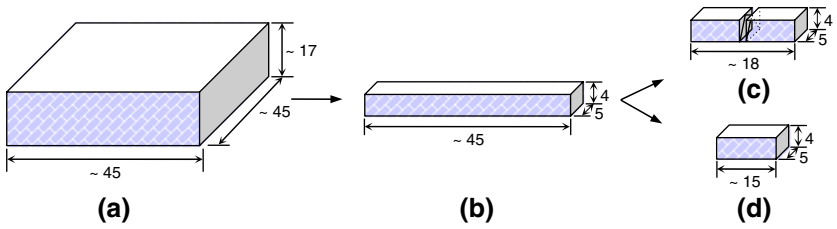

Fig. 1 Samples for mechanical testing (**a**) original block sample, (**b**) four-point bend testing sample, (**c**) Tattersall–Tappin testing sample, and (**d**) compressive testing sample

remains of the samples were prepared for Tattersall–Tappin fracture toughness testing and compression testing. Five to eight samples from each group were tested to obtain an average value for the mechanical strength. Four-point bending tests, work of fracture (Tattersall–Tappin testing) and compression tests were carried out using an Instron 1122 testing machine.

Four-point bend testing

The testing was carried out on rectangular bars with dimensions of $45 \times 5 \times 4$ mm which were sectioned from large block samples using a Buehler Isomet^{TM} 2000 Precision saw. The load and the rotational speed of the saw were 100–120 g and 3,600 rpm, respectively. Rough and chipped edges were ground off with silicon carbide paper. The samples were tested using an Instron 1122 testing machine with a cross-head speed of 0.5 mm/min; the span was 20 × 40 mm (Fig. 2). The four-point bend strengths (σ) were calculated using the equation:

$$\sigma \text{ (Pa)} = 3F(L - L_1)/2bd^2 \text{ (N/m}^2\text{)}$$

where

F = applied force,
L = the span of the support rollers,
L_1 = the separation of the loading span,
b = sample width,
d = sample thickness.

Work of fracture (Tattersall–Tappin test)

Rectangular bar samples approximately 18-mm long were cut from the remains of the samples used for four-point bending testing. Two cuts were made, using a diamond-wafering saw, to reduce the square cross-section to an isosceles triangular cross-section in the centre of the test piece. The chevron-shaped notched samples and the method of loading are shown in Fig. 3. This test required loading the notched specimen in three-point bending. The samples with dimensions of $18 \times 5 \times 4$ mm were loaded in the Instron 1122 test rig set on its most sensitive range, using a constant cross-head speed of 0.05 mm/min; the span was 15 mm. The apex of the triangular cross-section was placed in tension, thus causing a crack to initiate due to the extremely high stress concentration. This stress concentration meant that the crack was initiated at a load much lower than that required for complete catastrophic failure.

The work of fracture (J/m^2) was calculated by dividing the total work done (Nm) by the sum of the two areas of the triangular fracture surface (m^2). The equation used is as follows:

$$\text{Work of fracture (J/m}^2\text{)} = W/2A \text{ (Nm/m}^2\text{)}$$

where W (work done) is the area under the load–displacement curve. A is the area of the triangular crack face = wh/2.

Compressive testing

Compression test samples were made from the remains of those used for the four-point bend tests. Rectangular sections with an aspect ratio of in the order of 3:1 and dimensions of $15 \times 5 \times 4$ mm, were produced. This test required the top and the bottom of the samples to be flat

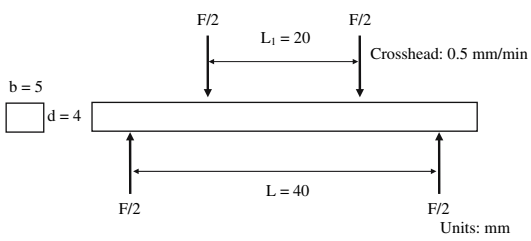

Fig. 2 Schematic drawing of the four-point bend testing

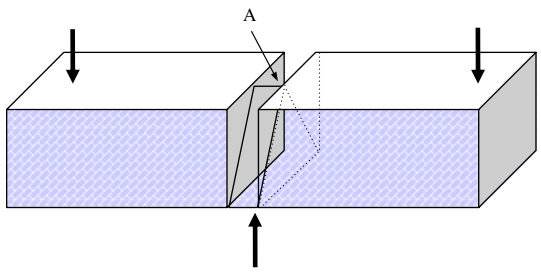

Fig. 3 Schematic diagram showing the shape of sample used to measure the work of fracture and the method of loading

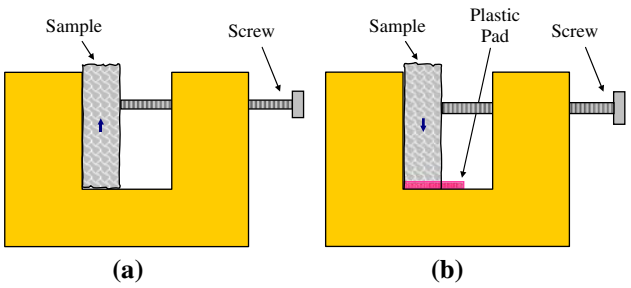

Fig. 4 A device for grinding samples for compressive testing (**a**) the sample is fastened in the gap by a screw and the top surface is ready to be ground (**b**) reversing the samples and inserting plastic pads under the sample allowed the opposite surface to be ground

and parallel so that the pressure was uniform on the surfaces and the force was applied parallel to the axis of the sample. Therefore, a device as shown in Fig. 4 was developed to enable the samples to be ground as flat as possible. Samples were fastened in the recess of the device by a screw. By adjusting the screw, various sizes of samples can be prepared. First, the top of the sample was ground flat; the sample was then reversed to allow the opposite surface to be similarly prepared. The holding jig allowed samples of different heights to be prepared by the use of a range of plastic pads employed to support the sample during grinding. Using the device, more accurate dimensions could be obtained.

Compressive tests were performed using an Instron 1122 materials testing machine with polished steel compression cylinders. Compressive testing was carried out both with and without inserting rubber supports. This is illustrated in Fig. 5. For the test with inserted rubber supports, a thin layer of rubber was placed between each end of the sample and the loading plates of the machine. The aim was to reduce shear stress concentration on the ends of the samples which were loaded up to fracture with a constant cross-head speed of 2 mm/min. Compressive strength was calculated from the load–deformation curve, by the ratio of ultimate applied force and cross-sectional area of the specimen.

Compressive strength is calculated by the equation:

$$\sigma\ (\mathrm{Pa}) = F/A\ (\mathrm{N/m^2})$$

where

σ is compressive stress,
F = applied force,
A = the specimen cross-sectional area.

Results and discussion

Porous calcium phosphate

Image analysis revealed the macroporosity levels measured for three different PU foams were similar and in the range of 5.24–9.67%. The macropore size of the HA/TCP bioceramics was in the range of 197–254 μm (for 20 ppi foam), 143–182 μm (for 30 ppi foam) and 105–135 μm (for 45 ppi foam). A typical example of the macroporosity visible on the surface of the samples is illustrated in Fig. 6(a). The average microporosities were found to be 15.07 ± 1.02%, 14.09 ± 0.84% and 4.23 ± 0.45% for the samples made from slips of solid loadings of 60, 100 and 120 wt%, respectively. A scanning electron micrograph

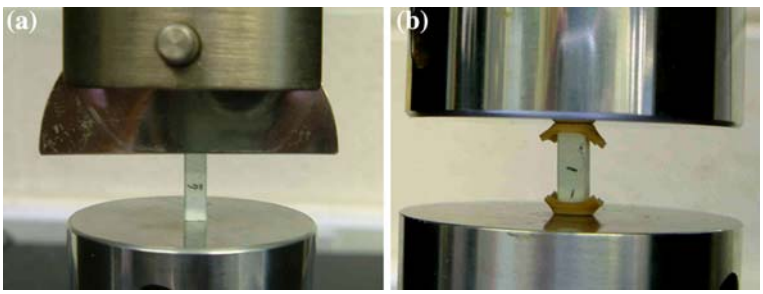

Fig. 5 Compressive testing (**a**) without inserting rubbers (**b**) with inserted rubber supports

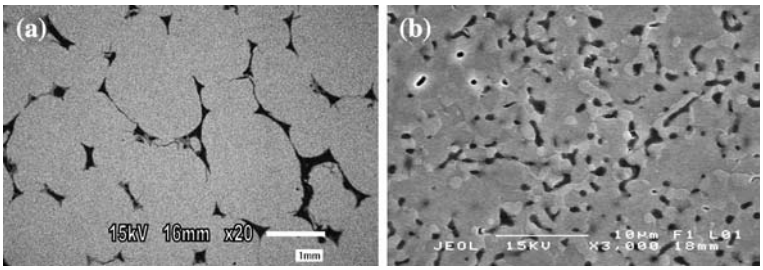

Fig. 6 Sample produced from 20 ppi foam with a slip loading of 100 wt% solid showing (**a**) macropores and (**b**) micropores

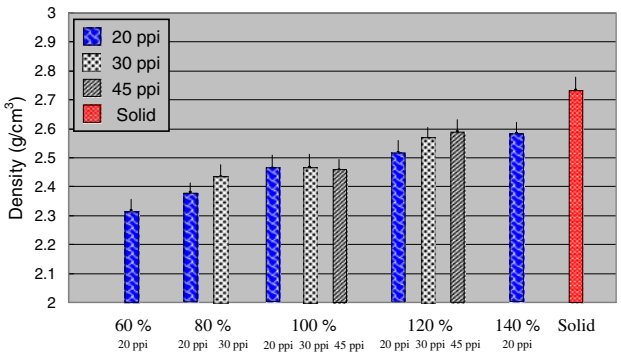

Fig. 7 The apparent density measurements of solid and porous blocks of the sintered HA/TCP bioceramics

illustrating the typical appearance of the microporosity is shown in Fig. 6(b).

Physical and mechanical properties

Density

Figure 7 and Table 2 show the apparent density of the solid sample (2.73 ± 0.05 g/cm^3) compared to the densities of the porous blocks of the sintered HA/TCP with different solid loading of slips and the theoretical densities of dense HA, β-TCP and α-TCP [13, 14].

Apparent density in relation to solid loading. The apparent density of the porous HA/TCP bioceramics fabricated by the vacuum impregnation technique was in the range of 2.32–2.59 g/cm^3. The densities of the porous samples increased with solid loading for each grade of foam. This can be explained in terms of the slips with higher solid loadings producing lower levels of microporosity.

Apparent density in relation to grade of foam. The densities produced from the different ppi foams are in the order of 20, 30 and 45 ppi from low to high. The only exception was the samples made from 100 wt% solid loading which had similar values of density irrespective of the grade of foam used as the initial template.

Table 3 shows the Student *t*-test results for the density measurements from solid and porous samples made from various solid loadings and ppi foams. The apparent density of the solid sample, made from the slip of 100 wt% solid loading, was highly significantly different to any of the other porous samples and was approximately 88% of the theoretical density. According to the Student *t*-test results, the differences in the apparent density between the porous samples made from the same grade of foam but different solid loadings were mostly significant or highly significant. The density of the samples was mostly the same and possibly different for 20, 30 and 45 ppi samples with a specific slip loading. From these results it can be seen that not only solid loading, but also the ppi of the foam, affected the apparent densities of porous samples. However, the grade of foam did not seem to have as great an effect on apparent density as the solid loading.

Table 2 The apparent densities of porous blocks of the sintered HA/TCP and the theoretical densities of HA, β-TCP, α-TCP

	The apparent densities (g/cm^3)		
Solid loading (wt%)	20 ppi	30 ppi	45 ppi
60	2.32 ± 0.04	–	–
80	2.38 ± 0.03	2.43 ± 0.04	–
100	2.46 ± 0.05	2.47 ± 0.05	2.46 ± 0.04
120	2.52 ± 0.04	2.56 ± 0.04	2.59 ± 0.04
140	2.58 ± 0.04	–	–
*Solid (slip cast)		2.73 ± 0.05	
The theoretical densities (g/cm^3)			
HA		β-TCP	α-TCP
3.16		3.07	2.86

Four-point bend testing

Figure 8 and Table 4 show the four-point bend testing results for solid and porous HA/TCP samples.

Four-point bend strength in relation to solid loading. Comparing the porous samples made from 20 ppi foam but different solid loading slips, there was no obvious relationship between four-point bend strengths and solid loading. Similar observations could be seen in samples made from 30 ppi foam. Samples made from 45 ppi foam with 120 wt% solid loading slip had slightly higher four-point bend strengths than those made from 100 wt% solid loading. This illustrated that microporosity did not have a profound effect on four-point bend strengths especially for samples which have larger macropores. In all cases, the scale of the microporosity could be below the critical flaw size for failure in four-point bend testing.

Four-point bend strength in relation to grade of foam. In general, irrespective of the solid loading, the four-point bend strength increased with the increase in the ppi of the foam precursor. The 45 ppi foam produced samples with the highest strength and the 20 ppi foam resulted in the lowest strength. This showed that macropore size had a noticeable effect on four-point bend strength thus the ppi of the starting foam structures had more effect than the actual solid loading.

The solid samples had the highest strengths which were in the order of 54.67 ± 5.83 MPa. In contrast, the average four-point bend strengths for the porous samples were in the range of 13.03–22.03 MPa. Four-point bend strength values are sensitive to the presence of defects, especially

Table 3 Student *t*-test results for the densities of solid and porous samples from various solid loadings and ppi foams

Solid loading (wt%)		60	80		100			120			140	Solid sample
	Foam (ppi)	20	20	30	20	30	45	20	30	45	20	
60	20		X	XX	XX	XX	XX	XX	XX	XX	XX	XX
80	20	X		#	X	X	X	XX	XX	XX	XX	XX
	30	XX	#		O	O	O	X	XX	XX	XX	XX
100	20	XX	X	O		O	O	#	XX	XX	XX	XX
	30	XX	X	O	O		O	#	XX	XX	XX	XX
	45	XX	X	O	O	O		#	XX	XX	XX	XX
120	20	XX	XX	X	#	#	#		□	#	#	XX
	30	XX	XX	XX	XX	XX	XX	□		O	O	XX
	45	XX	XX	XX	XX	XX	XX	#	O		O	XX
140	20	XX	XX	XX	XX	XX	XX	#	O	O		XX
Solid sample		XX	XX	XX	XX	XX	XX	XX	XX	XX	XX	

XX = Highly significant difference
X = Significant difference
# = Probable difference
□ = Possible difference
O = Difference not established

on the surface of the materials, so the strengths of the porous HA/TCP were considerably lower and inherently more variable. Table 5 shows the Student *t*-test results for the four-point bend strengths from solid and porous samples with various solid loadings and ppi foams. Unsurprisingly, the four-point bend strengths of porous samples were all highly significantly lower than that of the solid sample. The difference in four-point bend strengths between the porous samples made from the same grade of foam but different solid loadings were generally significantly different although in some cases there was no difference. However, the four-point bend strengths of the porous samples showed no particular order in relation to solid loading. Overall, the results showed that the different grades of starting foam had a noticeable effect on four-point bend strengths, in that the samples with a larger macropore size had lower four-point bend strengths. In contrast, the micropore sizes and level of microporosity did not seem to have a significant effect on the values of four-point bend strength.

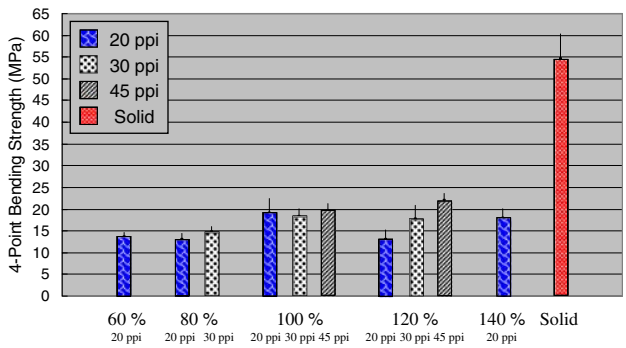

Fig. 8 The four-point bend strengths of the solid and porous sintered HA/TCP bioceramic

Table 4 The four-point bend strengths of solid and porous blocks of sintered HA/TCP bioceramics

	4-point bend strength (MPa)		
Solid loading (wt%)	20 ppi	30 ppi	45 ppi
60	13.74 ± 1.07	–	–
80	13.03 ± 1.42	14.82 ± 1.23	–
100	19.20 ± 3.22	18.32 ± 1.81	19.65 ± 1.75
120	13.16 ± 2.17	17.84 ± 3.15	22.03 ± 1.76
140	17.98 ± 2.18	–	–
*Solid (slip cast)		54.67 ± 5.83	

The average four-point bending strength for porous calcium phosphate bioceramics fabricated by the vacuum impregnation technique was 16.98 MPa (range: 13.03–22.03 MPa). With one exception, the bending strengths quoted in the literature by other authors, carried out by either four-point bend or three-point bend tests, are below 11 MPa [15–17] which is significantly lower than that for the porous samples produced in this project. The highest bending strength of porous calcium phosphate ceramics in the literature is ~40 MPa [18] which is much higher than that of the samples made by vacuum impregnation technique in the current research project. It may be that the interconnected porosity in the samples in the current project may encourage crack growth resulting in lower bending strengths than quoted in this one paper [18]. However, it can be seen that the strengths achieved were significantly higher than the majority of the figures quoted in the literature.

Work of fracture (Tattersall–Tappin testing)

A key feature of the Tattersall–Tappin test is that the cross-head speed should be sufficiently low to allow cracks to

Table 5 Student *t*-test results for the four-point bend strengths of solid and porous samples from various solid loadings and ppi foams

Solid loading (wt%)		60	80		100			120			140	Solid sample
	Foam (ppi)	20	20	30	20	30	45	20	30	45	20	
60	20		O	O	X	XX	XX	O	#	XX	X	XX
80	20	O		#	X	XX	XX	O	X	XX	XX	XX
	30	O	#		#	X	XX	O	□	XX	#	XX
100	20	X	X	#		O	O	#	O	O	O	XX
	30	XX	XX	X	O		O	X	O	X	O	XX
	45	XX	XX	XX	O	O		XX	O	#	O	XX
120	20	O	O	O	#	X	XX		#	XX	X	XX
	30	#	X	□	O	O	O	#		#	O	XX
	45	XX	XX	XX	O	X	#	XX	#		X	XX
140	20	X	XX	#	O	O	O	X	O	X		XX
Solid sample		XX	XX	XX	XX	XX	XX	XX	XX	XX	XX	

XX = Highly significant difference
X = Significant difference
# = Probable difference
□ = Possible difference
O = Difference not established

grow, rather than the sample to fail catastrophically, otherwise very variable results will be recorded. Figure 9 shows the load–deflection curve of the test with too high a cross-head speed. The sample broke immediately after the applied force exceeded the yield strength and the resulting curve was totally different to the ideal curve in Fig. 10. The highest force is at the end of the testing not in the middle of the testing. A typical curve for Tattersall–Tappin testing is shown in Fig. 10. The load verses deflection curve is linear before fracture begins (AB). When a crack is initiated the load falls. The region BC corresponds to rapid crack extension. The crack continues to grow in a controlled manner (CD). The cross-head speed should be low enough to allow crack growth in the sample during the tests. Figure 11 and Table 6 show the results of Tattersall–Tappin testing of solid and porous HA/TCP samples.

Work of fracture in relation to grade of foam and solid loading. For all the different grades of foam, the work of fracture generally increased with the increase in solid loading. Comparing the results from different foams, the work of fracture, measured from lowest to the highest, correlated with the increase in ppi. This trend was observed for 80, 100 and 120 wt% solid-loading slips. Samples made from 30 and 45 ppi foams with 100 wt% had similar values for work of fracture but the samples made from 45 ppi foam still had a higher value than the samples made from 30 ppi foam. The results showed similar trends to those observed for the measurement of density, four-point bend test and compressive tests. This is most likely the result of the different macropore sizes present in the samples.

Table 7 shows the Student *t*-test results for the work of fracture from solid and porous samples from various solid loadings and ppi foams. The results indicated that the solid

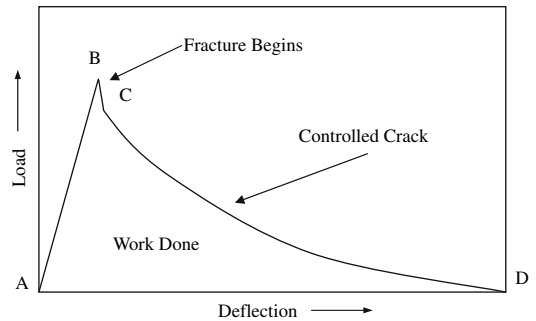

Fig. 10 Typical load–deflection curve for a Tattersall–Tappin test

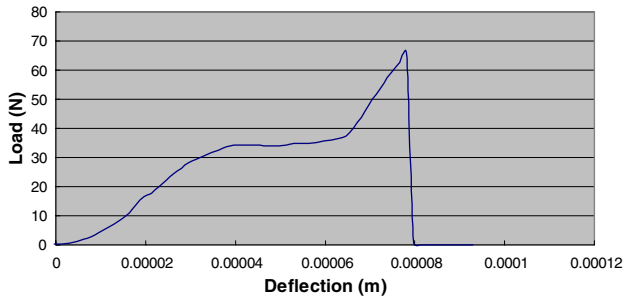

Fig. 9 The load–deflection curve of Tattersall–Tappin testing with too fast a cross-head speed

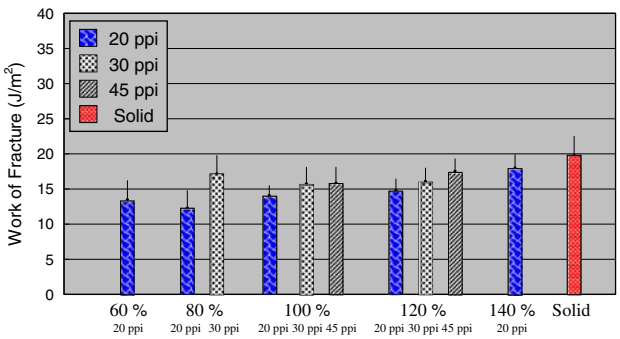

Fig. 11 Results of Tattersall–Tappin testing for solid and porous HA/TCP bioceramic

Table 6 The work of fracture of solid and porous blocks of sintered HA/TCP bioceramics

	Work of fracture (J/m^2)		
Solid loading (wt%)	20 ppi	30 ppi	45 ppi
60	13.50 ± 2.69	–	–
80	12.23 ± 2.52	17.17 ± 2.69	–
100	13.99 ± 1.60	15.71 ± 2.39	15.80 ± 2.35
120	14.71 ± 1.76	16.04 ± 2.04	17.49 ± 1.93
140	17.98 ± 1.98	–	–
*Solid (slip cast)		19.72 ± 1.93	

sample has the highest work of fracture but relatively, the difference when compared to the porous samples, is not as great as in the measurements from other mechanical tests. According to the Student *t*-test results, the differences in the work of fracture between the porous samples made from the same grade of foam but different solid loading are not significant and only a few of them show a significant or highly significant difference. The work of fracture of the porous samples is largely the same with some possible difference for 20, 30 and 45 ppi samples with a specific slip loadings. The results showed that work of fracture was slightly influenced by solid loading of slip and the grade of foam. Samples with a larger macropore size had a lower work of fracture and the work of fracture also increased with solid loading. However, the differences between the porous samples made from various ppi foams and solid-loading slips were relatively low compared to other mechanical tests. This may be because the Tattersall–Tappin test is not as sensitive to low levels of porosity.

The results show that the work of fracture was slightly influenced by solid loading of slip and the foam structure. Samples with larger macropore sizes had lower values for work of fracture. However, the standard deviations in each group tested were high and particularly so when compared to the results from other mechanical tests.

The average value of work of fracture for the porous calcium phosphate bioceramics fabricated by the vacuum impregnation technique was 15.46 J/m^2 (range: 12.23–17.98 J/m^2). Few results for the work of fracture for calcium phosphate can be found in the literature. The only data reported for calcium phosphate based ceramics are dense HA samples reinforced with Ti particles and dense calcium phosphate reinforced with fibres. Their values for work of fracture are 12.8 J/m^2 [19] and 1.5–3.5 $\times$ 10^3 J/m^2 [20], respectively. However, these values for work of fracture are significantly different to each other probably as a result of the different reinforcement mechanisms. Both of the tests were carried out on dense samples without notches which are not directly comparable with the porous samples made by the vacuum impregnation technique in this study. According to the literature [21, 22], the work of fracture values might be affected by the notch depth ratio (*h*/*w*).

Compressive testing

In order to reduce shear stress concentrations, a thin layer of rubber was inserted between each end of the sample and the loading plate of the machine during compressive tests as shown in Fig. 5. The difference between testing without inserting rubbers and testing with the inserted rubber supports can be seen in Fig. 12. The tests carried out with the rubber inserted resulted in higher compressive strengths and similar gradient curves in the elastic deformation region. This demonstrated that inserting the rubbers ensured more consistent results. The compressive strengths of solid and porous HA/TCP samples are shown in Fig. 13 and Table 8.

Table 7 Student *t*-test results for the work of fracture of solid and porous samples from various solid loadings and ppi foams

Solid loading (wt%)		60	80		100			120			140	Solid sample
	Foam (ppi)	20	20	30	20	30	45	20	30	45	20	
60	20		O	O	O	O	O	O	O	#	X	X
80	20	O		#	O	#	#	□	#	X	XX	XX
	30	O	#		□	O	O	O	O	O	O	O
100	20	O	O	□		O	O	O	O	#	X	X
	30	O	#	O	O		O	O	O	O	□	#
	45	O	#	O	O	O		O	O	O	□	#
120	20	O	□	O	O	O	O		O	#	X	X
	30	O	#	O	O	O	O	O		O	O	#
	45	#	X	O	#	O	O	#	O		O	O
140	20	X	XX	O	X	□	□	X	O	O		O
Solid sample		X	XX	O	X	#	#	X	#	O	O	

XX = Highly significant difference
X = Significant difference
# = Probable difference
□ = Possible difference
O = Difference not established

Compressive strength in relation to solid loading. Comparing the samples made from 20 ppi foams but with different solid loadings, the compressive strength increased slightly with the solid loading except in 80 wt% solid loading. This trend could also be seen in the samples made from 30 ppi foams. The samples made from 45 ppi foams had similar values of compressive strength for the slips with 100 and 120 wt% solid loadings. These results showed that generally the compressive strengths increased slightly with the solid loading. In the initial experiment, the compressive strengths decreased significantly when the solid loading was higher than 100 wt%. This was due to the fact that the samples contained many cracks when the slip had such a high solid loading. However, subsequently, it was found that the compressive strengths could be increased slightly when the solid loading was over 100 wt% by reducing the viscosity of the slip and extending the drying duration. This demonstrated that solid loading had an effect on compressive strength and higher solid-loading results in higher compressive strengths.

Compressive strength in relation to grade of foam. Comparing the samples made from the same solid loading but different ppi foams, the strengths from low to high are in the order of 20, 30 and 45 ppi foams. This shows macropores have an influence on compressive strength and larger macropore sizes resulted in a lower compressive strengths.

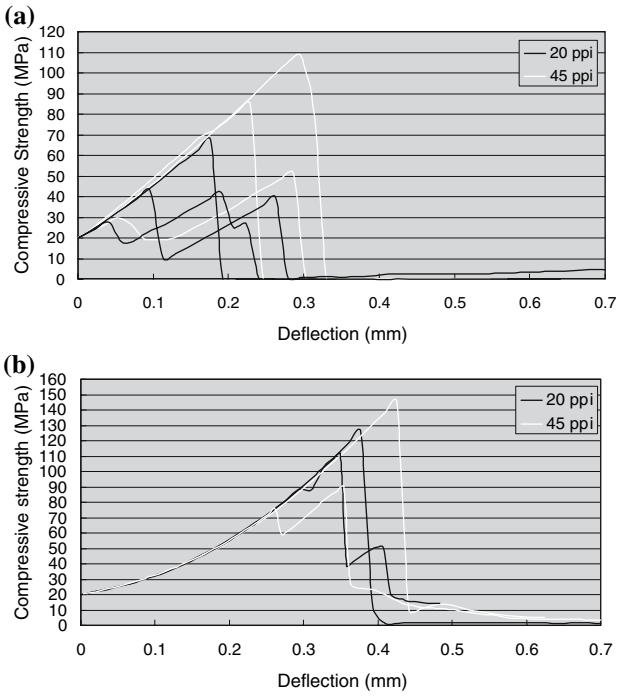

Fig. 12 Results of compressive testing (**a**) without inserting rubbers (**b**) with inserted rubber supports

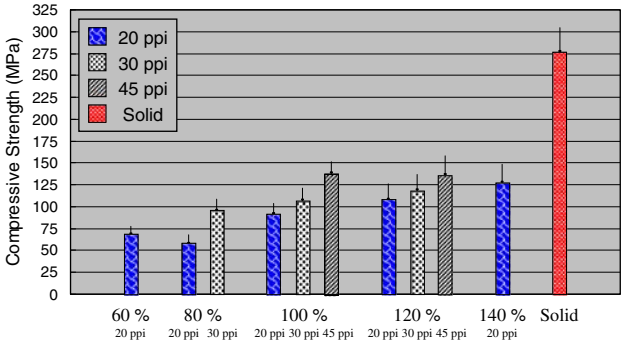

Fig. 13 Compressive strengths of the solid and porous sintered HA/TCP bioceramic

The average compressive strengths for porous sample were in the range of 58.46–138.72 MPa. The solid samples had the highest compressive strength, which was 277.79 ± 26.97 MPa. Table 9 shows the Student *t*-test results for the compressive strengths of solid and porous samples made from various solid loadings and ppi foams. According to the Student *t*-test results, the compressive strength of the solid sample, made from the slip of 100 wt% solid loading, was highly significantly different to any other porous samples. The differences in the compressive strength of the porous samples made from the same grade of foam, but different solid loadings varied from no difference to a significant difference. The effect of foam size on compressive strength was similar to that of solid loading on compressive strength. The differences in the compressive strength between the porous samples made from the same solid loading, but different grades of foam varied from no difference to a significant difference. It can be seen that the compressive strengths were influenced by not only foam structures, but also solid loading. Samples with larger macropore sizes and microporosities had lower compressive strengths.

Table 8 The compressive strength of solid and porous blocks of sintered HA/TCP bioceramics

Solid loading (wt%)	Compressive strength (MPa)		
	20 ppi	30 ppi	45 ppi
60	68.90 ± 9.03	–	–
80	58.46 ± 9.35	96.00 ± 12.73	–
100	92.00 ± 12.12	107.51 ± 13.75	138.72 ± 12.58
120	109.00 ± 17.17	119.46 ± 16.97	137.20 ± 20.73
140	128.30 ± 19.95	–	–
*Solid (slip cast)		277.79 ± 26.97	

Table 9 Student *t*-test results for the compressive strengths of solid and porous samples from various solid loadings and ppi foams

Solid loading (wt%)		60	80		100			120			140	Solid sample
	Foam (ppi)	20	20	30	20	30	45	20	30	45	20	
60	20		O	□	□	X	XX	#	X	X	X	XX
80	20	O		#	#	X	XX	X	X	X	X	XX
	30	□	#		O	O	X	O	O	□	O	XX
100	20	□	#	O		O	X	O	O	#	□	XX
	30	X	X	O	O		X	O	O	#	O	XX
	45	XX	XX	X	X	X		#	O	O	O	XX
120	20	#	X	O	O	O	#		O	□	O	XX
	30	X	X	O	O	O	O	O		O	O	XX
	45	X	X	□	#	#	O	□	O		O	XX
140	20	X	X	O	□	O	O	O	O	O		XX
Solid sample		XX	XX	XX	XX	XX	XX	XX	XX	XX	XX	

XX = Highly significant difference
X = Significant difference
# = Probable difference
□ = Possible difference
O = Difference not established

The majority of the values for compressive strength of porous calcium phosphates reported in the literature are in the range 0.2–18 MPa [5, 11, 17, 23–26] and the highest is ~36 MPa [27]. As such, the porous samples in the literature would not be useful for substantial load-bearing applications. In contrast, the samples made by the vacuum impregnation technique used in the current research which were in the range of 58.46–138.72 MPa, were far in excess of any figures quoted in the literature, and as such could be used in a diversity of load-bearing applications.

Ideally, fracture of samples in compression testing will be caused by maximum shear stresses and the fracture surfaces in the sample will be oriented at the angle of 45° to the axes of loading. Although inserting rubber supports at each end of the sample can reduce stress concentrations and result in higher compressive strengths, the failure mode observed was not the classic shear failure expected at 45° along the axis. This phenomenon can be seen in Fig. 14 which illustrates the failure modes observed in both the solid and porous samples. The most common failure modes were fracture in the centre and at the corners of the samples. However, in both common failure modes the fracture lines in these samples were oriented parallel to the axes of loading.

According to literature [28], one explanation could be the friction between the sample and compression platens. The literature also mentioned that if the interface is dry, leading to high friction between the samples and loading plate, then the fracture surfaces in the sample, in this situation, will be oriented at an angle of 45° to the axes of loading. If the interface is oily or wet, allowing some sliding along the interface in the transverse direction, then fracture will be caused by transverse strains arising during loading. The fracture line in the sample will be oriented parallel to the axes of loading. However, in the current study, the interface was dry. The samples might have experienced some sliding along the interface in the transverse direction when the test was carried out without inserting rubber supports. However, using the rubber supports, the friction between the samples and the surface of the platens should be increased, reducing the tendency to slip.

In contrast to this, it was reported [29, 30] that friction could contribute to a measurement error and the platens need to be lubricated. When a sample is compressed, most types of material will expand in the transverse direction due to the Poisson's effect. Friction at the interface will interfere with this expansion and change the apparent

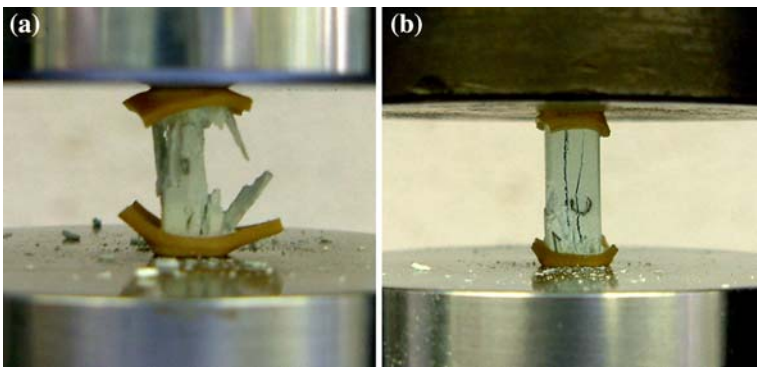

Fig. 14 Illustration of the common failure modes observed during compression testing in (**a**) porous samples and (**b**) solid samples

stiffness of the sample. Further work needs to be carried out on the failure mode to find out if friction is the cause of the unexpected failure modes observed.

Conclusions

To date, porous calcium phosphates which combine interconnected porosity with good mechanical strengths have not been reported. In this study, Porous HA/TCP bioceramics with interconnected porosity combined with good mechanical properties were fabricated successfully by a novel technique of vacuum impregnation of reticulated polymeric foams with ceramic slip. The vacuum impregnation method can be used successfully to produce porous HA/TCP bioceramics with both regular and irregular three-dimensional shapes. The samples have an excellent porous structure without isolated pores. Nearly 100% of the macroporosity arises from the PU foam template. The macropore sizes produced in this research were larger than 100 μm in diameter which is appropriate for bone ingrowth.

Comparing the results obtained in the current study with the mechanical strengths of porous calcium phosphate published in the literature indicates that it is possible to manufacture open pore HA/TCP bioceramics with mechanical strengths exceeding these recorded for existing porous calcium phosphate ceramics. The porous HA/TCP samples made by the vacuum impregnation technique may have much more potential for substantial load-bearing applications which could be of clinical interest.

Acknowledgements The authors would like to thank the University of Bath and Stryker Howmedica Osteonics for their support.

References

1. L. L. HENCH, *J. Am. Ceram. Soc*. **81** (1998) 1705
2. L. L. HENCH, *J. Am. Ceram. Soc*. **74** (1991) 1487
3. A. TAMPIERI, G. CELOTTI, S. SPRIO, A. DELCEGLIANO and S. FRANZESE, *Biomaterials* **22** (2001) 1365
4. T. M. G. CHU, D. G. ORTON, S. J. HOLLISTER, S. E. FEINBERG and J. W. HALLORAN, *Biomaterials* **23** (2002) 1283
5. J. TIAN and J. TIAN, *J. Mater. Sci*. **36** (2001) 3061
6. B. FLAUTRE, M. DESCAMPS, C. DELECOURT, M.C. BLARY and P. HARDOUIN, *J. Mater. Sci.: Mater. Med*. **12** (2001) 679
7. J. X. LU, B. FLAUTRE, K. ANSELME and P. HARDOUIN, *J. Mater. Sci.: Mater. Med*. **10** (1999) 111
8. J. H. KUHNE, R. BARTL, B. FRISH, C. HANMER, V. JANSSON and M. ZIMMER, *Acta Orthopaedica Scand*. **65** (1994) 246
9. P. S. EGGLI, W. MULLER and R. K. SCHENK, *Clin. Orthopaedics Related Res*. **232** (1988) 127
10. V. KARAGEORGIOU and D. KAPLAN, *Biomaterials* **26** (2005) 5474
11. R. P. REAL, J. G. C. WOLKE, M. VALLET-REGI and J. A. JANSEN, *Biomaterials* **23** (2002) 3673
12. Y. H. HSU, I. G. TURNER and A. W. MILES, *Key Eng. Mater*. **284–286** (2005) 305
13. J. D. SANTOS, J. C. KNOWLES, R. L. REIS, F. J. MONTEIRO and G. W. HASTING, *Biomaterials* **15** (1994) 5
14. R. A. YOUNG and J. C. ELLIOT, *Arch. Oral Biol*. **11** (1966) 699
15. M. MILOSEVSKI, J. BOSSERT, D. MILOSEVSKI and N. GRUEVSKA, *Ceram. Int*. **25** (1999) 693
16. N. O. ENGIN and A. C. TAS, *J. Eur. Ceram. Soc*. **19** (1999) 2569
17. M. FABBRI, G. C. CELOTTI and A. RAVAGLIOLI, *Biomaterials* **16** (1995) 225
18. D. M. LIU, *Ceram. Int*. **24** (1998) 441
19. C. CHU, P. LIN, Y. DONG, X. XUE, J. ZHU and Z. YIN, *J. Mater. Sci.: Mater. Med*. **13** (2002) 985
20. H. H. K. XU and J. B. QUINN, *Biomaterials* **23** (2002) 193
21. R. W. DAVIDGE and G. TAPPIN, *J. Mater. Sci*. **3** (1968) 165
22. L. A. SIMPSON, *J. Am. Ceram. Soc*. **56** (1972) 7
23. P. SEPULVEDA, J. G. P. BINNER, S. O. ROGERO, O. Z. HIHA and J. C. BRESSIANI, *J. Biomed. Mater. Res*. **50** (2000) 27
24. K. A. HING, S. M. BEST and W. BONFIELD, *J. Mater. Sci.: Mater. Med*. **10** (1999) 135
25. P. SEPULVEDA, F. S. ORTEGA, M. D. M. INNOCENTINI and V. C. PANDOLFELLI, *J. Am. Ceram. Soc*. **83** (2000) 3021
26. H. R. RAMAY and M. ZHANG, *Biomaterials* **24** (2003) 3293
27. D. M. LIU, *Ceram. Int*. **23** (1997) 135
28. Y. H. AN. and R. A. DRAUGHN (eds), *Mechanical Testing of Bone and the Bone-Implant Interface* (CRC Press, London, 2000)
29. S. C. COWIN (ed) *Bone Mechanics Handbook* (CRC Press, New York, 2001) pp. 7–9
30. M. KISER, M. Y. HE and F. W. ZOK, *Acta Mater*. **47** (1999) 2685